Journal of the Serbian Society for Computational Mechanics / Vol. 14 / No. 2, 2020 / pp 133-149
(10.24874/jsscm.2020.14.02.09)

INVESTIGATING POSSIBILITIES OF CRACK INITIATION LIFE EXTENSION IN JET ENGINES COMPRESSOR DISKS

Strain Posavljak[1*], Gordana Tosic[2], Katarina Maksimovic[3]

[1] University of Banja Luka, Faculty of Mechanical Engineering, 71 Vojvode Stepe Stepanovica Street, 78000 Banja Luka, Republic of Srpska, Bosnia and Herzegovina
E-mail: strain.posavljak@mf.unibl.org
[2] University of Banja Luka, Faculty of Mechanical Engineering, 71 Vojvode Stepe Stepanovica Street, 78000 Banja Luka, Republic of Srpska, Bosnia and Herzegovina
E-mail: gordana.tosic@mf.unibl.org
[3] Secretariat for Utilities and Housing Services Water Management, 1 Kraljice Marije Street, Belgrade, Serbia
E-mail: kmaksimovic@mts.rs
**corresponding author*

Abstract

This paper deals with jet engines compressor disks which have dovetail joints with blades. A compressor disk with reduced fatigue resistance was taken as an example. Two simplified conceptual solutions of the dovetail joint with blades were devised. Based on the low cycle fatigue theory, the crack initiation life of their critical parts with newly-proposed transition rounding at the bottom of dovetail grooves was estimated. Two different flank angles in the dovetail grooves (60° in the critical part that belongs to the first dovetail joint conceptual solution and 55° in the critical part that belongs to the second dovetail joint conceptual solution), two different aviation steels selected for workmanship (13H11N2V2MF and AISI 304 steel) and two load histories (load history LH1 and load history LH2), were taken into account. By load history LH2 an overload of the critical parts was simulated. The results of crack initiation life estimation of the critical parts in the dovetail joint conceptual solutions show that there is a possibility for the crack initiation life extension of the observed compressor disk. In all analyzed variants, it has been shown that the critical part in the second dovetail joint conceptual solution has longer crack initiation life than the critical part in the first dovetail joint conceptual solution. For example, the critical part in the second dovetail joint conceptual solution made of AISI 304 steel, in the case of load history LH1 has 141.55% longer crack initiation life than the critical part in the first dovetail joint conceptual solution made of 13H11N2V2MF steel. In the case of load history LH2 (an overload case) that percent is greater and amounts to 173.15%.

Keywords: Jet engines, compressor disks, dovetail joints, crack initiation, life extension.

1. Introduction

During exploitation, jet engine compressors and turbine disks are exposed to low cycle fatigue. Their service life observed as crack initiation life is limited and prescribed by jet engines

producers. In practice, it can happen that the prescribed service life of some disks is not reached (Posavljak, 2008). The reasons for this can be different, such as poorly chosen geometry, inadequate surface quality, the disk material has bad cyclic properties, inadequate spin tests, overload in operation and, finally, the lack of exact crack initiation life assessment methods.

As a result of loads in the form of their own centrifugal forces, centrifugal forces of blades, gas-dynamic forces, plus elevated temperature, "premature" cracks can be caused in the stressed areas of disks, due to the appearance of increased elasto-plastic strains. The stressed areas of jet engine disks are rims, areas with holes of different purposes and hubs. Here, interesting rims are stressed because of joint with blades. In many cases, crack initiation life of disks is determined by the quality of these joints.

The typical joint of the compressor's disks with blades is dovetail joint, for which interest has not ceased. For example, Shlyannikov, Yarullin and Ishtyryakov (2019), Stepovoy and Pribora (2018) and Kozakiewicz, Grzejszczak and Lacki (2017) have analyzed different ways, jet engine compressor disks and their dovetail joints with blades.

2. Case of one jet engine compressor disk and its dovetail joint with blades

2.1 Introductory information

The existing first stage low pressure compressor disk of R25–300 jet engine, here observed as disk D1, has a dovetail joint with blades. The service life of 1200 flight hours of this disk, made of 13H11N2V2MF steel, has never been reached because of "premature" cracks which appeared in the region of the transition rounding at the dovetail groove bottom. This fact is confirmed by Weibull's probability expression of cracks appearance that was established by Posavljak (2008), in the form:

$$P(t) = 1 - e^{-\left(\frac{t}{336}\right)^{2.764}} . \tag{1}$$

The diagram of this probability and a sample of disk D1 with discovered crack is presented in Fig. 1.

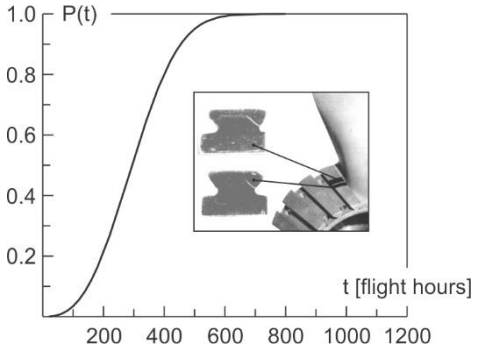

Fig. 1. Weibull's probability diagram of crack appearance and a sample of disk D1 with discovered crack

The practical crack initiation life of disk D1 for the probability 0.001 amounts to 27.6 flight hours and for the probability 0.999 it amounts to 676.1 flight hours.

Posavljak (2008) proved that the existing transition rounding at the dovetail grooves bottom in disk D1 needs to be replaced by the new transition rounding if we want to extend the crack initiation life. New transition rounding, better than the existing, was proposed for disk D2 that represents the second version of the first stage low pressure compressor disk of R25-300 jet engine, made of 13H11N2V2MF steel in the heat treatment state (heating at 1000 °C, oil quenching, tempering at 640°C and air cooling). The existing and newly-proposed transition rounding can be seen in Fig. 2.

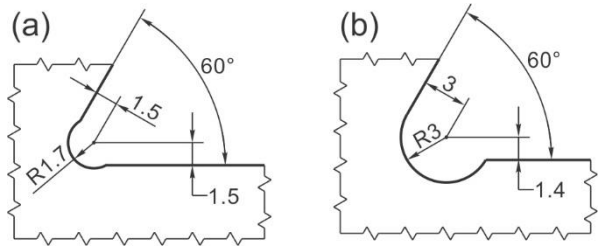

Fig. 2. Transition rounding at the dovetail groove bottom of disk D1 (a) and newly-proposed transition rounding for disk D2 (b)

Newly-proposed transition rounding shown in Fig. 2b will be kept in two conceptual dovetail joint solutions that will be discussed here. The task is to discover the other possibilities of crack initiation life extension of the first stage low pressure compressor disk of R25-300 jet engine and accordingly to this, to suggest its third version marked as disk D3.

2.2 Conceptual dovetail joint solutions

The joints with blades of the first stage low pressure compressor disk of R25-300 jet engine, as dovetail joints, are simplified here. The first conceptual dovetail joint solution, with identified main parts (lower and upper part), is shown in Fig. 3.

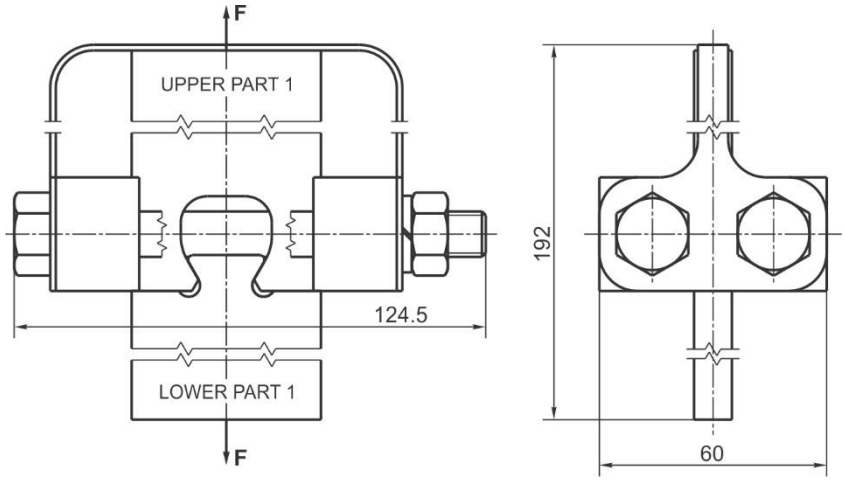

Fig. 3. The first conceptual dovetail joint solution with identified main parts (the lower and upper part)

The second conceptual dovetail solution is not shown here, as it is similar to the first. Taking into consideration dimensionally defined lower parts LP1 and LP2 (Fig. 4) and upper parts UP1 and UP2 (Fig. 5), the difference between our two conceptual dovetail joint solutions can be noticed.

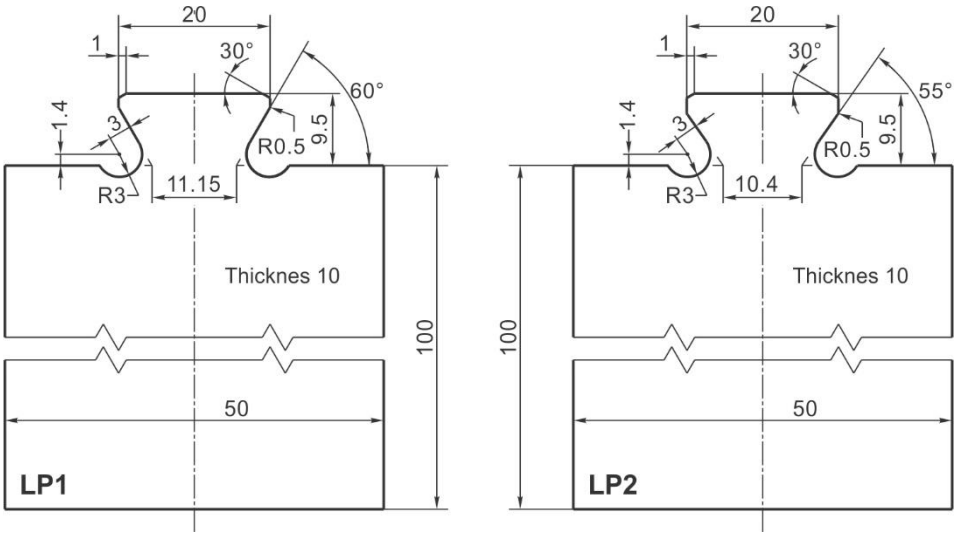

Fig. 4. The lower parts LP1 and LP2 of the first and the second conceptual dovetail joint solution

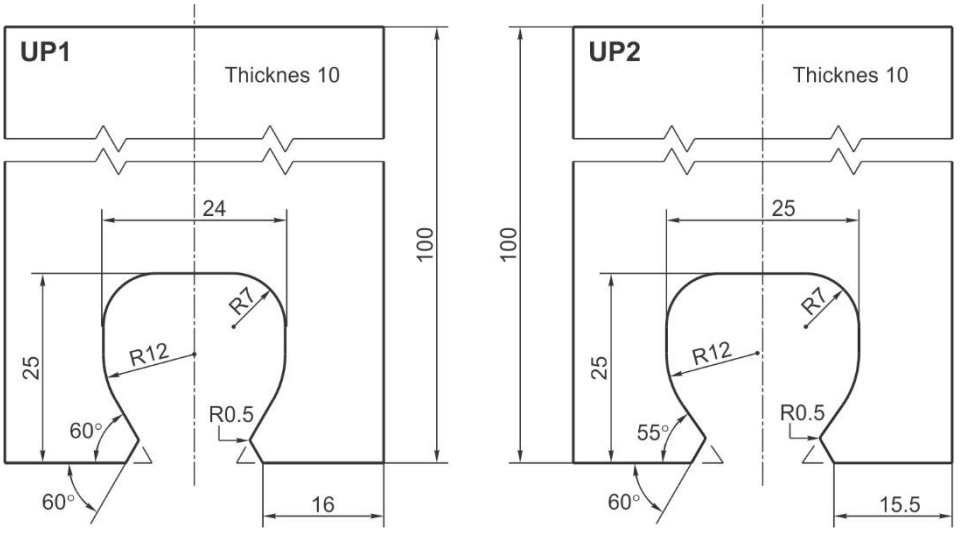

Fig. 5. The upper parts UP1 and UP2 of the first and the second conceptual dovetail joint solution

2.3 Fatigue properties of materials selected for the main parts workmanship of dovetail joint conceptual solutions

Two aviation steels, 13H11N2V2MF steel (S1 steel) in the above mentioned heat treatment state and AISI 304 steel (S2 steel), were selected for the main parts workmanship of conceptual dovetail joint solutions.

Fatigue properties of 13H11N2V2MF steel, experimentally in the regime of controlled strains, obtained by Posavljak (2008) and fatigue properties of AISI 304 steel taken from SAE J1099 (2002), are presented in Table 1.

Property	13H11N2V2MF steel (S1 steel)	AISI 304 steel (S2 steel)
Modulus of elasticity, E [MPa]	229184.6	190000
Cyclic strength coefficient, K′ [MPa]	1140	2275
Cyclic strain hardening exponent, n′	0.0579	0.334
Fatigue strength coefficient, σ'_f [MPa]	1557.3	1267
Fatigue strength exponent, b	–0.0851	–0.139
Fatigue ductility coefficient, ε'_f	0.3175	0.174
Fatigue ductility exponent, c	–0.7214	–0.415

Table 1. Fatigue properties of 13H11N2V2MF steel and AISI 304 steel

2.4 Load histories of observed dovetail joints

Assuming that dovetail joints would be exposed to the load histories LH1 and LH2 that shown in Fig. 6. These histories include positively variable force *F*. By the load history LH2 an overload of 10% will be simulated.

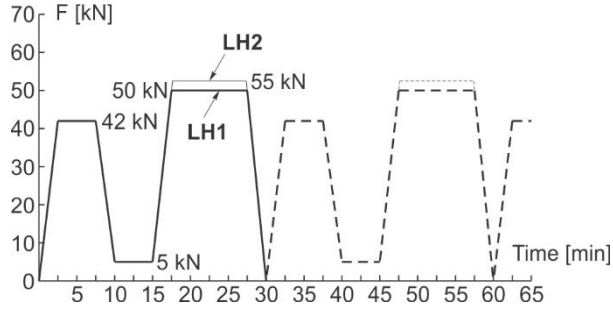

Fig. 6. Load histories LH1 and LH2

Fig. 7 shows the shortened array of simplified load history LH1. Applying the method of "reservoir", as Kostaes (2001) did, the force cycles 50-0-50 kN and 42-5-42 kN were identified in that array.

In the similar way, 55-0-55 kN and 42-5-42 kN force cycles would be identified in the shortened array of simplified load histories LH2.

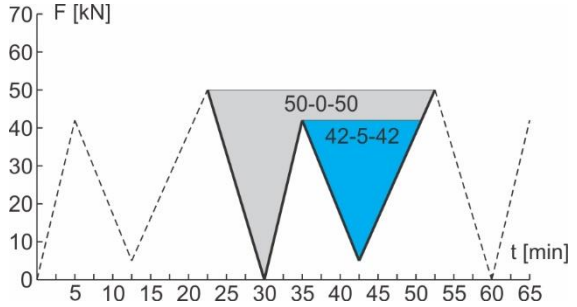

Fig. 7. The shortened array of simplified load histories LH1 with identified force cycles

2.5 Local stress-strain response of the critical dovetail joint parts

The critical parts of the dovetail joints are the lower parts LP1 and LP2. They belong to a group of notched structural elements. At the first step, the linear stress response will be obtained (the case of ideal elasticity). This stress response will serve to identify critical points in those lower parts (points with maximum values of principal stresses σ_1). After that, the values of corresponding nominal stresses σ_n and theoretical stress concentration factors K_t will be determined. In the end, the values of σ_n and K_t will be used for the computation of nonlinear stress-strain response (the case of elasto-plasticity).

Taking into account the steels selected, S1 and S2 will be added to the basic marks LP1 and LP2 of the lower parts, practically performing the task with four lower parts: LP1S1, LP1S2, LP2S1 and LP2S2.

Linear stress response. For the purpose of the linear stress response computation of the lower parts LP1 and LP2, the computational models were formed, as shown in Fig. 8.

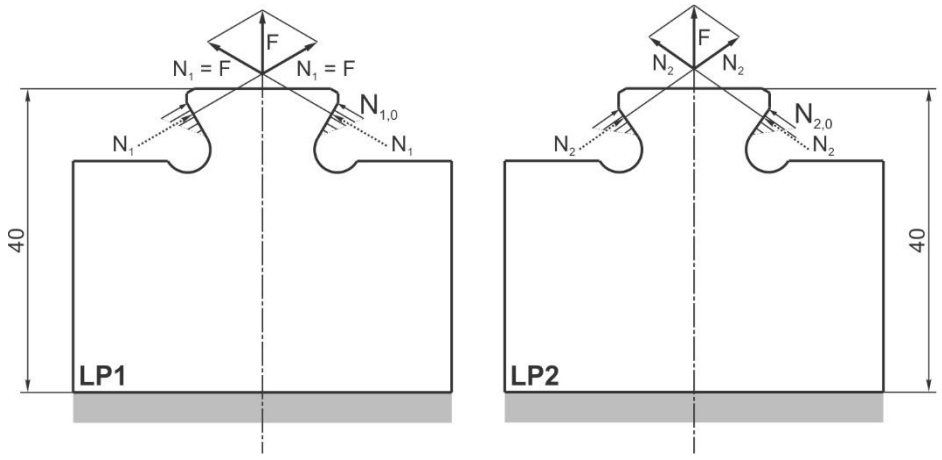

Fig. 8. Computational models of the lower parts LP1 and LP2

The influence of the upper parts UP1 and UP2, as can be seen in the previous figure, was compensated by distributing normal forces N_1 and N_2 along the contact lines. The values of these normal forces can be obtained using the following expressions:

$$N_1 = \frac{F}{2\cos 60°}$$
$$N_2 = \frac{F}{2\cos 55°} \tag{2}$$

In both cases, the force F is the resultant of the normal forces N_1 and N_2.

After establishing the computational models shown in Fig. 8, using the finite element method (FEM) implemented in IDEAS Master Series 7 Software, FEM models of the lower parts LP1S1 and LP2S1 were generated (Fig. 9). The "plane stress parabolic" 8-noded finite element was used for discretization. For the generation of FEM models, the symmetry of given lower parts was used.

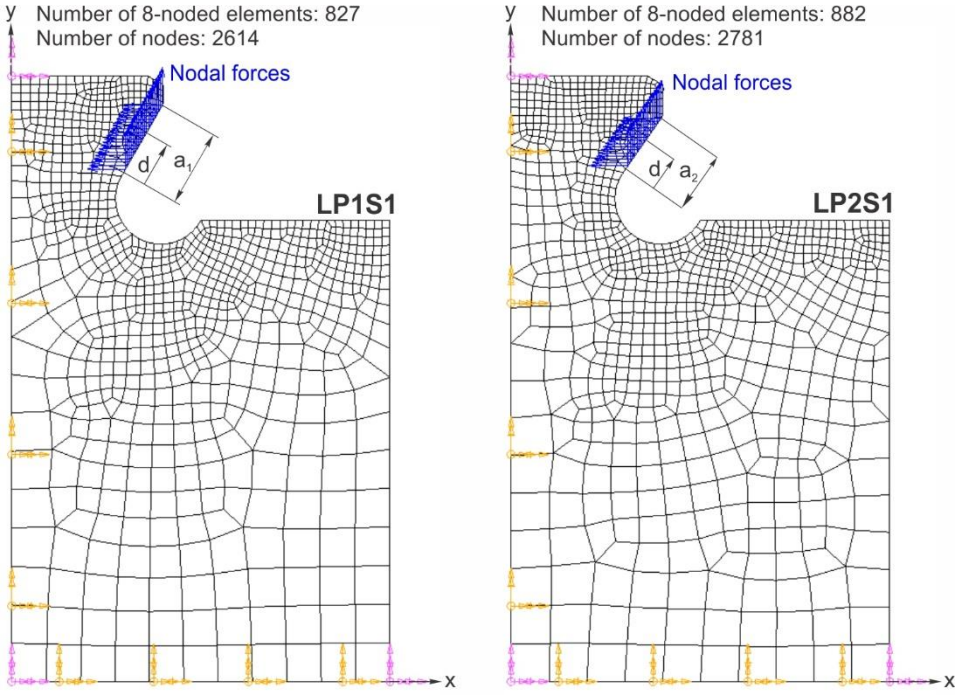

Fig. 9. FEM models of the lower parts LP1S1 and LP2S1

To all finite elements modulus elasticity $E = 2.291846\times10^8$ mN/mm^2, Poisson's coefficient $\nu = 0.29$, shear modulus $G = 8.883124\times10^7$ mN/mm^2 and mass density $\rho = 7.82\times10^{-6}$ kg/mm^3 (for steel 13H11N2V2MF, steel S1), were assigned. All finite elements were assigned the thickness of 10 mm as a physical property.

Boundary conditions connected with the FEM models of the observed lower parts are zero displacements for all nodes that belong to the x-axis, free vertical displacements for all nodes that belong to the y-axis (excluding node in the coordinate system origin), plus horizontal and vertical nodal forces.

The law of distribution of horizontal and vertical nodal forces is defined by the following expressions:

$$H_1(d) = -\frac{N_{1,0}}{a_1} d \sin 60°, \quad V_1(d) = \frac{N_{1,0}}{a_1} d \cos 60°$$
$$H_2(d) = -\frac{N_{2,0}}{a_1} d \sin 55°, \quad V_2(d) = \frac{N_{2,0}}{a_1} d \cos 55° \quad . \tag{3}$$

In these expressions the following can be noticed: normal nodal forces $N_{1,0}$ and $N_{2,0}$ at the end of contact lines, the lengths of contact lines a_1 and a_2 and d as distances of a certain nod from the nod at the start of contact lines. The forces $N_{1,0}$ = 4×10^6 mN and $N_{2,0}$ = 4.307×10^6 mN, correspond to the normal forces N_1 = 42×10^6 mN and N_2 = 36.612×10^6 mN when F = 42×10^6 mN (see Fig. 8). The lengths of contact lines amount to: a_1 = 5.079 mm and a_2 = 4.074 mm.

The isolines of principal stresses σ_1 in the segments of lower parts LP1S1 and LP2S1, with identified maximum stress values in the critical points P_1 and P_2, are shown in Fig.10.

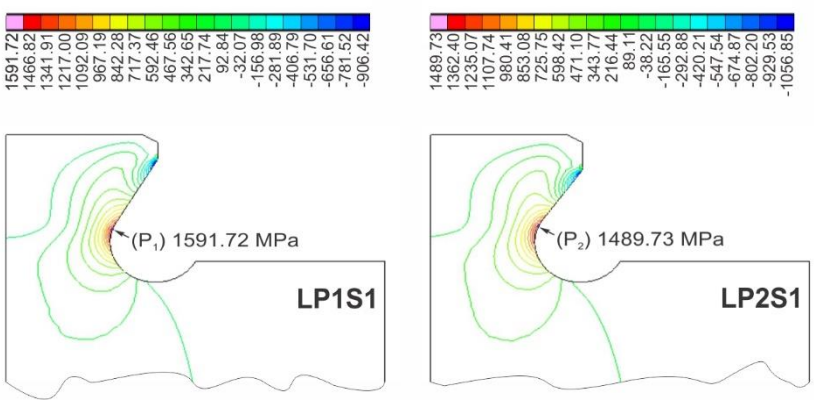

Fig. 10. The isolines of principal stresses σ_1 in the segments of lower parts LP1S1 and LP2S1, with identified maximum stress values in the critical points P_1 and P_2

The critical points P_1 and P_2 with stresses $\sigma_1(P_1)$ = 1591.72 MPa and $\sigma_1(P_2)$ = 1489.73 MPa, belong to critical sections with areas A_1 = 140.5 mm^2 and A_2 = 142.2 mm^2. By dividing the force F = 42×10^3 N, with these areas, nominal stresses were obtained, i.e. σ_{n1} = 298.932 MPa (for the lower part LP1) and σ_{n2} = 295.359 MPa (for the lower part LP2).

Theoretical (or geometrical) stress concentration factors K_{t1} = 5.325 (for the lower part LP1) and K_{t2} = 5.044 (for the lower part LP2) were computed by dividing stresses $\sigma_1(P_1)$ and $\sigma_1(P_2)$ with the above mentioned nominal stresses.

Note that the same maps of the principal stresses σ_1 that are shown in Fig. 10 can also be obtained for the lower parts LP1S2 and LP2S2.

The data about linear stress response in the critical points that belong to the critical sections of all lower parts, at the level of nominal stresses, are included in Table 2.

Lower part	Load history	k	Force cycle $F_{k,u}$-$F_{k,l}$-$F_{k,u}$ [kN]	Nominal stress cycle $\sigma_{nk,u}$-$\sigma_{nk,l}$-$\sigma_{nk,u}$ [MPa]	Nominal stress range $\Delta\sigma_{nk}$ [MPa]
LP1S1	LH1	1	50-0-50	355.871-0-355.871	355.871
		2	42-5-42	298.932-35.587-298.932	263.345
	LH2	3	55-0-55	391.459-0-391.459	391.459
		4	42-5-42	298.932-35.587-298.932	263.345
LP2S1	LH1	5	50-0-50	351.618-0-351.618	351.618
		6	42-5-42	295.359-35.162-295.359	260.197
	LH2	7	55-0-55	386.780-0-386.780	386.780
		8	42-5-42	295.359-35.162-295.359	260.197
LP1S2	LH1	9	50-0-50	355.871-0-355.871	355.871
		10	42-5-42	298.932-35.587-298.932	263.345
	LH2	11	55-0-55	391.459-0-391.459	391.459
		12	42-5-42	298.932-35.587-298.932	263.345
LP2S2	LH1	13	50-0-50	351.618-0-351.618	351.618
		14	42-5-42	295.359-35.162-295.359	260.197
	LH2	15	55-0-55	386.780-0-386.780	386.780
		16	42-5-42	295.359-35.162-295.359	260.197

Table 2. The data about linear stress response in the critical points that belong to the critical sections of all lower parts, at the level of nominal stresses

The values of already obtained nominal stress σ_{n1} = 298.932 MPa and σ_{n2} = 295.359 MPa are shown in Table 2. The first nominal stress is equal to the upper nominal stresses $\sigma_{nk,u}$ (k = 2,4,10,12) in the nominal stress cycles, while the second is also equal to the upper nominal stresses $\sigma_{nk,u}$ (k = 6,8,14,16) in the nominal stress cycles.

The other upper and lower nominal stresses in the nominal stress cycles were obtained by multiplying values of the mentioned nominal stresses with the quotient of corresponding force in the force cycles and force that amounts to 42 kN. The ranges of nominal stresses $\Delta\sigma_{nk}$ were obtained as difference of the upper $\sigma_{nk,u}$ and the lower $\sigma_{nk,l}$ nominal stresses values in the nominal stress cycles.

Local nonlinear stress-strain response. Local nonlinear stress-strain response of our lower parts refers to their critical points. Such a stress-strain response was determined by stabilized hysteresis loops (two stabilized hysteresis loops per load history).

The kth upper point $[(\Delta\varepsilon/2)_k, (\Delta\sigma/2)_k]$ of the kth main stabilized hysteresis loop that corresponds to the force cycles 50-0-50 kN in the load history LH1 and 55-0-55 kN in the load history LH2 was determined by solving the system of equations

$$\frac{\Delta\varepsilon}{2}=\frac{1}{2}\frac{K_{ti}\sigma_{nk,u}}{E_j}\left(\frac{K_{ti}\sigma_{nk,u}}{\frac{\Delta\sigma}{2}E_j}+1\right)$$
$$\frac{\Delta\varepsilon}{2}=\frac{1}{E_j}\left(\frac{\Delta\sigma}{2}\right)+\left[\frac{1}{K'_j}\left(\frac{\Delta\sigma}{2}\right)\right]^{\frac{1}{n'_j}} \quad (4)$$

in which the indexes i, j and k had these values: (i = 1, j = 1, k = 1,3), (i = 2, j = 1, k = 5,7), (i = 1, j = 2, k = 9,11) and (i = 2, j = 2, k = 13,15).

By solving the system of equations

$$\Delta\varepsilon = \frac{1}{2}\frac{K_{ti}\Delta\sigma_{nk}}{E_j}\left(\frac{K_{ti}\Delta\sigma_{nk}}{\Delta\sigma E_j}+1\right)$$
$$\Delta\varepsilon = \frac{1}{E_j}(\Delta\sigma)+2\left[\frac{1}{K'_j}\left(\frac{\Delta\sigma}{2}\right)\right]^{\frac{1}{n'_j}} \quad (5)$$

the dimension $\Delta\varepsilon_k \times \Delta\sigma$ of kth stabilized hysteresis loop was obtained.

The indexes i, j and k in (5) had these values: (i = 1, j = 1, k = 1,2,3,4), (i = 2, j = 1, k = 5,6,7,8), (i = 1, j = 2, k = 9,10,11,12) and (i = 2, j = 2, k = 13,14,15,16).

The upper points, of the stabilized hysteresis loops that correspond to the force cycles 42-5-42 kN belong to the main stabilized hysteresis loops. Their position, at the height $\Delta\sigma = \Delta\sigma'_k$, measured from the lower point of the main hysteresis loops, was obtained by introducing auxiliary 42-0-42 kN force cycle and by solving the system equations (5) for the cases when are: (i = 1, j = 1, k = 2,4), (i = 2, j = 1, k = 6,8), (i = 1, j = 2, k = 10,12) and (i = 2, j = 2, k = 14,16).

The first equations in the systems (4) and (5) are two forms of Birger-Sonsino's curve (Birger, 1985 and Sisino, 1993). The second equations in that systems are equations of the cyclic stress-strain curve and Massing's curve (for steel S1 if j =1 and steel S2 if j = 2). These curves are broadly described by Bannatine, Comer and Handrock (1990).

The stress concentration factors K_{ti} (i = 1,2) in Birger-Sonsino's curves had values of already determined stress concentration factors K_{t1} = 5.325 and K_{t2} = 5.044.

The values for E_j, K'_j and n'_j (j = 1,2) in the systems of equations (4) and (5) were taken from Table 1. Index j = 1 refers to steel 13H11N2V2MF (steel S1), while index j = 2 refers to steel AISI 304 (steel S2). The corresponding values of upper nominal stresses $\sigma_{nk,u}$ in nominal stress cycles, including stress ranges $\Delta\sigma_{nk}$, were taken from Table 2.

The systems of equations (4) and (5) were solved graphically in DRAFTING modulus of IDEAS Master Series 7 Software by Posavljak (2008). By the special programs generated in Visual FORTRAN, all curves were copied to corresponding spline curves.

Two examples of graphically determined nonlinear stress-strain responses in the critical points of the lower parts LP1S1 and LP1S2 exposed to load history LH1 are presented in Fig. 11 and Fig. 12.

Considering the strain memory of metals, the stabilized hysteresis loops (two per load history) were modelled using Massing's curve for steel S1 and steel S2.

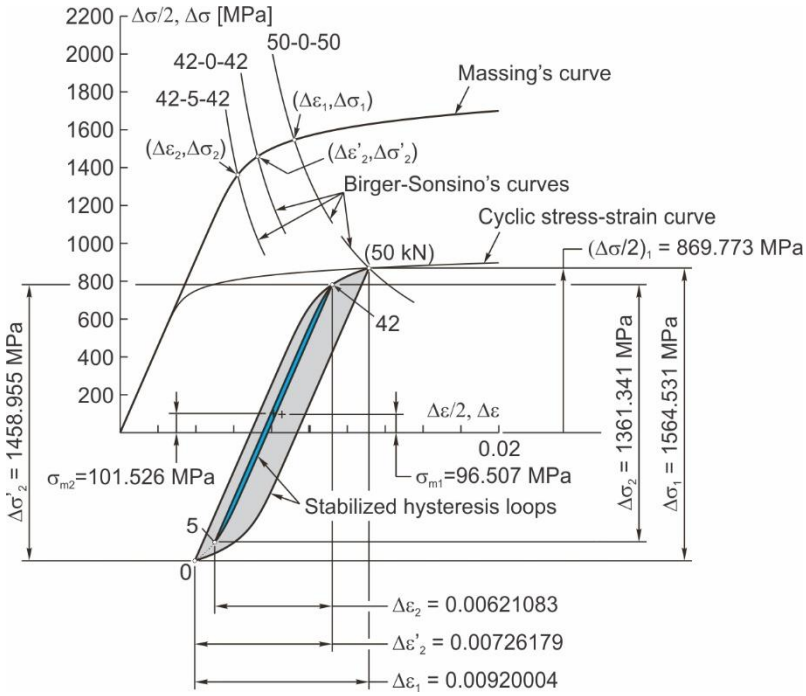

Fig. 11. Nonlinear stress-strain response in the critical point of the lower part LP1S1 exposed to the load history LH1

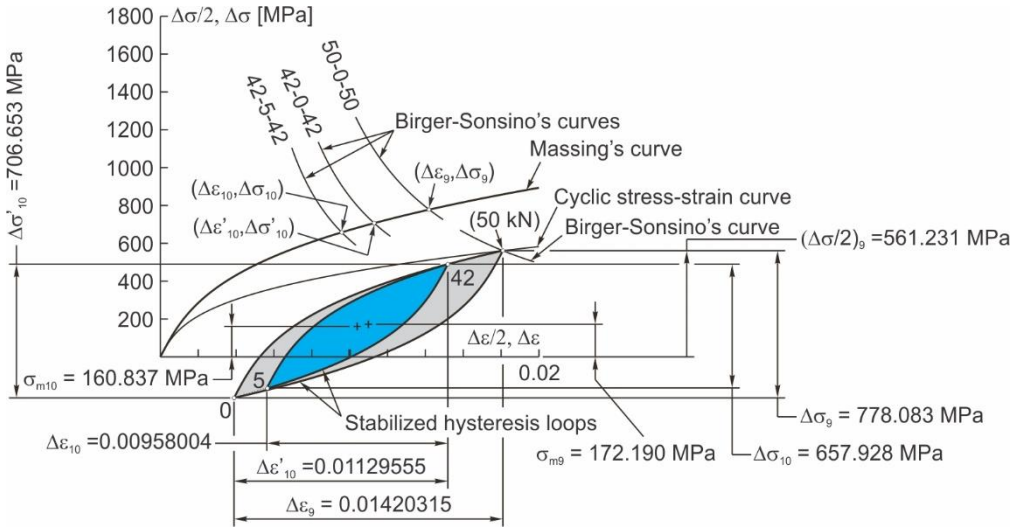

Fig. 12. Nonlinear stress-strain response in the critical point of the lower part LP1S2 exposed to the load history LH1

The set of numerical data on the nonlinear stress-strain response in the critical points of all lower parts exposed to load histories LH1 and LH2 is shown in Table 3.

Lower part	Load history	k	Force cycle $F_{k,u}$-$F_{k,l}$-$F_{k,u}$ [kN]	Mean stress σ_{mk} [MPa]	Strain range $\Delta\varepsilon_k$	Stress range $\Delta\sigma_k$ [MPa]	$(\Delta\sigma/2)_k$ [MPa]
LP1S1	LH1	1	50-0-50	96.507	0.00920004	1564.531	869.773
		2	42-5-42	101.526	0.00621083	1361.341	---
	LH2	3	55-0-55	89.076	0.01053913	1582.203	880.177
		4	42-5-42	76.259	0.00621083	1361.341	---
LP2S1	LH1	5	50-0-50	103.575	0.00839119	1517.593	862.372
		6	42-5-42	109.980	0.00576499	1259.030	
	LH2	7	55-0-55	93.948	0.00958561	1558.052	872.974
		8	42-5-42	80.123	0.00576499	1295.030	---
LP1S2	LH1	9	50-0-50	172.190	0.01420315	778.083	561.231
		10	42-5-42	160.837	0.00958004	657.928	---
	LH2	11	55-0-55	179.668	0.01611625	819.441	589.389
		12	42-5-42	147.636	0.00958004	657.928	---
LP2S2	LH1	13	50-0-50	167.213	0.01301527	750.323	542.374
		14	42-5-42	156.184	0.00879543	633.470	
	LH2	15	55-0-55	174.431	0.01476007	790.519	569.690
		16	42-5-42	143.304	0.00879543	633.470	---

Table 3. The set of numerical data on the nonlinear stress-strain response in the critical points of all lower parts exposed to the load histories LH1 and B2

2.6 Damages and crack initiation life estimation

Damages and crack initiation life estimation here was based on Palmgren-Miner's rule developed by Palmgren (1924) and Miner (1945).

Damages estimation. The k[th] damage D_k of all lower parts, provoked by k[th] force cycle in the load histories LH1 and LH2, was computed using the expression

$$D_k = \frac{N_k}{N_{fk}}, \qquad k = 1,2,...,16 \tag{6}$$

in which $N_k = 1$ represents the number of k[th] force cycles in the load histories LH1 and LH2, while N_{fk} represents the number of accumulated k[th] force cycles to crack initiation (to failure) in the certain lower part of our dovetail joints.

The set of $N_f = N_{fk}$ data was obtained by solving the system of equations

$$\begin{aligned} \frac{\Delta\varepsilon}{2} &= \frac{\sigma'_{f,j} - \sigma_{mk}}{E_j} N_f^{b_j} + \varepsilon'_{f,j} N_f^{c_j} \\ \frac{\Delta\varepsilon}{2} &= \frac{\Delta\varepsilon_k}{2} \end{aligned} \tag{7}$$

in which the indexes j and k had the next values: (j = 1, k = 1,2,3,4,5,6,7,8) and (j = 2, k = 9,10,11,12,13,14,15,16). The values of k[th] mean stresses σ_{mk} and k[th] strain range $\Delta\varepsilon_k$ in that system were taken from Table 3.

The first equation in the system (7) is the equation of Morrow's strain-life curve of steel S1 if j = 1 and steel S2 if j = 2. This curve, suggested by Morrow (1968) and applied by Bannantine, Comer an Handrock (1990), represents one of the modifications of the basic strain-life curve.

Posavljak (2008) and after that Maksimovic, Posavljak and other (2011) has shown that by using Morrow's curves in combination with Birger-Sonsino's curves, satisfying results of crack initiation life estimation can be obtained in comparison with experimental results.

The system of equations (7) was also solved graphically. The set of Morrow's curves was copied to the corresponding set of spline curves.

The data about N_k, $N_f = N_{fk}$, and D_k that refer to all observed lower parts exposed to the load histories LH1 and LH2 are shown in Table 4. The example of graphical determined accumulated numbers of force cycles 50-0-50 in the load history LH1 (N_{f1} and N_{f9} in Table 4) to the crack initiation in the lower parts LP1S1 and LP1S2 is shown in Fig. 13.

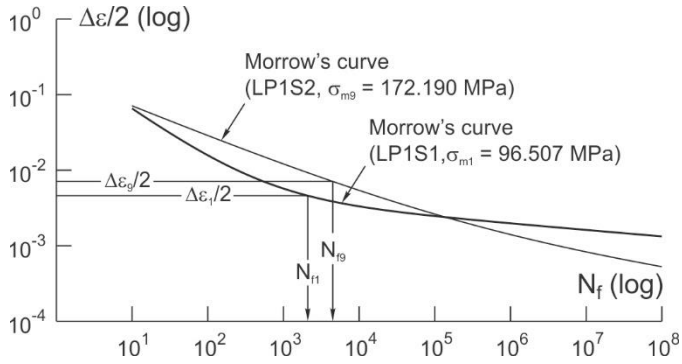

Fig. 13. Example of graphical determined accumulated numbers of force cycles 50-0-50 in the load history LH1 (N_{f1} and N_{f9}) to crack initiation in the lower parts LP1S1 and LP1S2

Lower parts	Load history	k	Force cycle $F_{k,u}$-$F_{k,l}$-$F_{k,u}$ [kN]	N_k	N_{fk}	Damage $D_k = N_k / N_{fk}$
LP1S1	LH1	1	50-0-50	1	2096	0.00047710
		2	42-5-42	1	15175	0.00006590
	LH2	3	55-0-55	1	1309	0.00076394
		4	42-5-42	1	16889	0.00005921
LP2S1	LH1	5	50-0-50	1	2995	0.00033389
		6	42-5-42	1	24894	0.00004017
	LH2	7	55-0-55	1	1806	0.00055371
		8	42-5-42	1	28812	0.00003471
LP1S2	LH1	9	50-0-50	1	4482	0.00022311
		10	42-5-42	1	14588	0.00006855
	LH2	11	55-0-55	1	3103	0.00032227
		12	42-5-42	1	14762	0.00006774
LP2S2	LH1	13	50-0-50	1	5800	0.00017241
		14	42-5-42	1	19069	0.00005244
	LH2	15	55-0-55	1	4005	0.00024969
		16	42-5-42	1	19304	0.00005180

Table 4. N_k, N_{fk} and D_k data for all lower parts exposed to the load histories LH1 and LH2

Using the data about damages D_k contained in Table 4, damages $D_{k,k+1}$ for all lower parts, caused by the load histories LH1 and LH2, were obtained. For that purpose, we used the expression

$$D_{k,k+1} = D_k + D_{k+1}, \quad k = 1,3,5,7,9,11,13,15 . \tag{8}$$

Crack initiation life estimation. The results of crack initiation life (CIL) estimation of all lower parts exposed to the load histories LH1 and LH2 were obtained using the expression

$$CIL_{k,k+1} = 0.5 \times \frac{1}{D_{k,k+1}}, \quad k = 1,3,5,7,9,11,13,15 . \tag{9}$$

The results of estimated damages and estimated crack initiation life of all observed lower parts in the case of exposition to the load histories LH1 and LH2 are shown in Table 5.

Lower part	Load history	Damage caused by load history		CIL [Hours]	
		Mark	Value	Mark	Value
LP1S1	LH1	$D_{1,2}$	0.00054300	$CIL_{1,2}$	920.5
	LH2	$D_{3,4}$	0.00082315	$CIL_{3,4}$	607
LP1S2	LH1	$D_{5,6}$	0.00029166	$CIL_{5,6}$	1714
	LH2	$D_{7,8}$	0.00039001	$CIL_{7,8}$	1282
LP2S1	LH1	$D_{9,10}$	0.00037406	$CIL_{9,10}$	1336.5
	LH2	$D_{11,12}$	0.00058842	$CIL_{11,12}$	849.5
LP2S2	LH1	$D_{13,14}$	0.00022485	$CIL_{13,14}$	2223.5
	LH2	$D_{15,16}$	0.00030149	$CIL_{15,16}$	1658

Table 5. The results of estimated damages and estimated crack initiation life (CIL) of all observed lower parts in the case of exposition to the load histories LH1 and LH2

3. Results comparison of crack initiation life estimation

The results comparison of crack initiation life estimation, of the lower parts LP1S1, LP2S1, LP1S2 and LP2S2, here are presented by corresponding histograms.

The overload of 10% covered by the load history LH2, in the same lower parts of our dovetail joints, causes a significant drop of crack initiation life (Fig. 14). For LP1S1 34.06%, for LP1S2 25.20%, for LP2S1 36.44% and for LP2S2 25.43%.

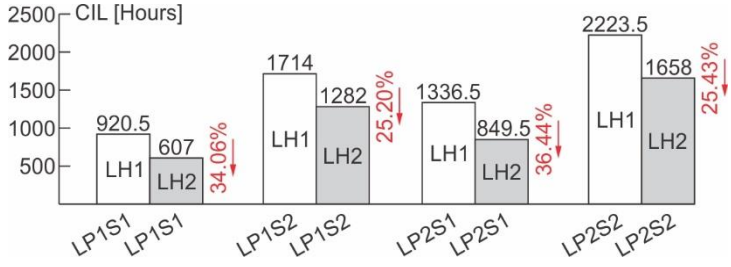

Fig. 14. Histogram of crack initiation life (CIL) comparison of the same lower parts exposed to the load histories LH1 and LH2

CIL of the lower parts LP1S2 and LP2S2, in comparison to CIL of the lower LP1S1 and LP2S1, for the case of exposure to the same load histories, is significantly higher (Fig. 15). The AISI 304 steel (S2 steel) with cyclic properties is prevailing.

Practically, the lower part LP1S2 has 86.20% greater CIL than the lower part LP1S1 in the case of exposure to load histories LH1, and 111.20% greater in the case of exposure to load histories LH2.

The lower part LP2S2 has 66.37% greater CIL than the lower part LP2S1 in the case of exposure to load histories LH1, and 95.17% greater in the case of exposure to load histories LH2.

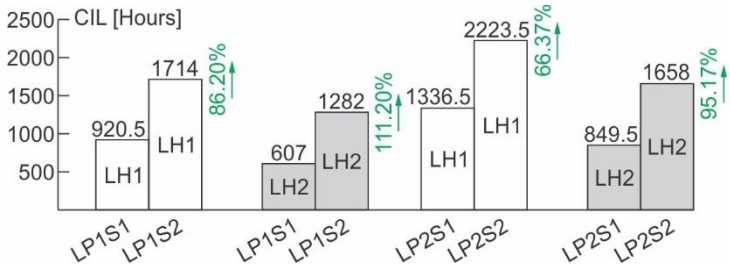

Fig. 15. Histogram of crack initiation life (CIL) comparison of the lower parts LP1S1, LP1S2, LP2S1 and LP2S2 exposed to the load histories LH1 and LH2

CIL of the lower parts LP2S1 and LP2S2 in comparison with CIL of the lower parts LP1S1 and LP1S2, for the case of exposure to the same load histories, has also increased (Fig. 16). The increase is a consequence of flank angle change from 60° to 55°.

The lower part LP2S1 has 45.15% greater CIL than the lower part LP1S1 in the case to exposure to load histories LH1, and 39.95% greater in the case of exposure to load histories LH2.

The lower part LP2S2 has 29.73% greater CIL than the lower part LP1S1 in the case of exposure to load histories LH1, and 29.33% greater in the case of exposure to load histories LH2.

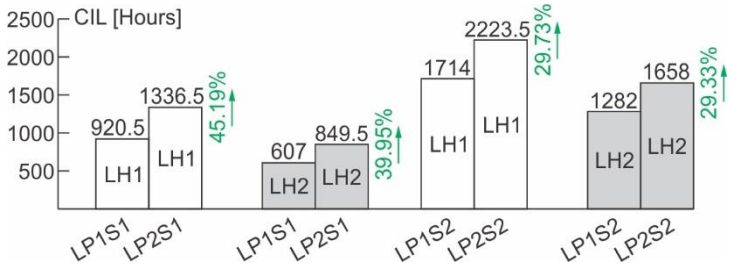

Fig. 16. Histogram of crack initiation life (CIL) comparison of the lower parts LP1S1, LP1S2, LP2S1 and LP2S2 exposed to the load histories LH1 and LH2

As can be seen in Fig. 17, the lower part LP2S2 has a distinctly greater CIL in comparison to the CIL of the lower part LP1S1, for the case of exposure to the same load histories. Here the flank angle change from 60° to 55°, together with steel change, is dominant (141.55% and 173.15%, in favor of the lower part LP2S2).

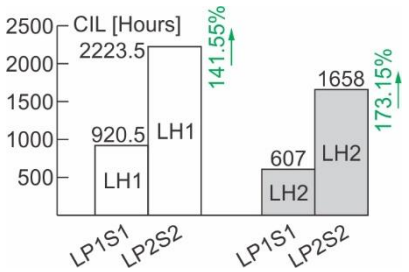

Fig. 17. Histogram of crack initiation life (CIL) comparison of the lower parts LP1S1, LP2S2 exposed to the load histories LH1 and LH2

4. Conclusions

On the basis of the above-presented results, the possibilities of crack initiation life extension of the first stage low pressure compressor disk of R25-300 jet engine have been discovered. The first possibility refers to the application of a flank angle of 55° in its joints with blades, dovetail joints. That angle is better than the flank angle of 60°. The second possibility refers to AISI 304 steel that needs to be chosen because it has better resistance to low cycle fatigue than 13H11N2V2MF steel in the defined heat treatment state. The best, third possibility combines the previous two possibilities.

Therefore, for the first stage low pressure compressor disk of R25-300 jet engine, the third version can be proposed. This version has been marked as disk D3, that would be made of AISI 304 steel and that would have dovetail grooves with newly-proposed transition rounding at the bottom and with the flank angles of 55°. The crack initiation life of disk D3 would be longer than crack initiation life of disk D2 that would be made of 13H11N2V2MF steel and would have dovetail grooves with newly-proposed rounding at the bottom and flank angles of 60°.

References

Bannantine J A, Comer J and Handrock J (1990). *Fundamentals of Material Fatigue Analysis*, Prentice-Hall, Englewood Cliffs, New Jersey.

Birger I A (1985). Prognozirovanie resursa pri malociklovoj ustalosti, *Problemy prochnosti*, No 10, 39-44.

Kostaes D (1994). Fatigue Behaviour and Analysis, Talat Lecture 2401, Technishe Universitat Munchen, European Aluminium Association – EAA.

Kozakievisz A, Grzejszczak O and Lacki T (2017). Numerical and Experimental Analysis of Compressor's Jet Engine Blade Joint Including the Model Parameterization, *Mechanik*, Vol. 90, No. 7, 562–564.

Maksimovic S, Posavljak S, Maksimovic K, Nikolic V, Djurkovic V (2011). Total Fatigue Life Estimation of Notched Structural Components Using Low-Cycle Fatigue Properties, *Strain*, Volume 47, Issue Supplement s2, 341-349.

Miner M A (1945). Cumulative Damage in Fatigue, *Journal of Applied Mechanics*, 76, A159-164.

Morrow J (1968). Fatigue Design Handbook, *Advances in Engineering*, Vol. 4, Society of Automotive Engineers, Warrendale, Pa., Sec. 3.2, 21-29.

Palmgren A (1924). Die Lebensdauer von Kugellagern, *Verfahenstechnik*, Berlin, 68, 339-341

Posavljak S (2008). *Fatigue Life Investigation of Aero Engine Rotating Disks* (in Serbian), Doctoral Dissertation, University of Belgrade, Faculty of Mechanical Engineering.

SAE J1099 (2002). Technical Report on Low Cycle Fatigue Properties Ferrous and Non-ferrous Materials, Society of Automotive Engineers, Inc.

Shlyannikov N, Yarulin R and Istyryakov S (2019). Failure Analysis of an Aircraft GTD Compressor Disk on the Base of Imitation Modeling Principles, *Procedia Structural Integrity* 18, 322–329.

Sonsino C M (1993). Zur Bewertung Schwingfestigkeitsverhaltens von Bauteilen mit Hilife Örtlicher Beanspruchungen, *Konstrukcion*, 45, 25-33.

Stepovoy S, Pribora I (2018). Analiz Evolyucii Konstrukcii Zamkovogo Soedineniya Rabochih Koles Kompressorov GTD, *Vestnik dvigatelestroenija*, No. 1, 53–59.